This document is the accepted manuscript version of the following article:
Pandiyan, V., Drissi-Daoudi, R., Shevchik, S., Masinelli, G., Le-Quang, T., Logé, R., & Wasmer, K. (2021). Semi-supervised monitoring of laser powder bed fusion process based on acoustic emissions. Virtual and Physical Prototyping. https://doi.org/10.1080/17452759.2021.1966166

Semi-supervised Monitoring of Laser Powder Bed Fusion Process Based on Acoustic Emissions

Vigneashwara Pandiyan [a], Rita Drissi-Daoudi [b], Sergey Shevchik [a], Giulio Masinelli [a], Tri Le-Quang [a], Roland Logé [b], Kilian Wasmer [a,*]

[a] *Laboratory for Advanced Materials Processing (LAMP), Swiss Federal Laboratories for Materials Science and Technology (Empa)-CH-3602 Thun, Switzerland*

[b] *Thermomechanical Metallurgy Laboratory – PX Group Chair, Ecole Polytechnique Fédérale de Lausanne (EPFL), CH-2002 Neuchâtel, Switzerland*

* Corresponding author. Tel.: +41-58-762-62-71; fax: +41-58-762-69-90. *E-mail address:* kilian.wasmer@empa.ch

Abstract

Metal-based Laser Powder Bed Fusion (LPBF) suffers from a lack of repeatability and is challenging to model, making their quality monitoring essential and demanding. The reason lies in the high dynamics taking place during the interaction of the laser with metallic powders. To bring this technology to mass production, industries are only interested in the process regime where the built layer's quality meets their standards. All other process regimes leading to poor mechanical properties and/or defect formation such as *balling, Lack of Fusion (LoF) pores, keyhole pores*, delamination, and crack propagation irrespective of their different regimes are considered anomalies. Today, the common methodology for monitoring uses conventional/supervised Machine Learning (ML) algorithms for the classification task requires collecting a balanced dataset corresponding to each investigated regime from the sensors, which is very expensive and time-consuming. As an alternative, the article proposes a semi-supervised approach where the defect-free regime can be differentiated from the anomalies by familiarising the ML algorithms only with the distribution of acoustic signatures corresponding to the defect-free regime. This work presents two generative Convolutional Neural Network architectures based on Variational Auto-Encoder and General Adversarial Network. As a result, we could classify the anomaly regimes with 96 and 97% accuracy, respectively.

Keywords: Laser powder bed fusion; Monitoring; Laser processing; Convolutional Neural Network; Acoustic Emission.

WORD COUNT: 9'411

1 Introduction

Laser Powder-Bed Fusion (LPBF) is one of the Additive Manufacturing (AM) techniques allowing the building of 3D complex geometries components from an alloy powder layer by layer (King et al. 2015). The main advantages of this technology are a considerable reduction of geometrical design constraints (Khairallah et al. 2016; Brandt 2016), lead-time optimization due to computer-aided design (CAD) (Guessasma et al. 2015), the possibility to use various powder materials, and last but not least revolutionize the production of spare parts in the supply chain (Khajavi, Partanen, and Holmström 2014). The major drawback of this technology is a deficiency in the process reproducibility and the lack of robust and economical process monitoring which impacts the mechanical properties (e.g., part density and grain structure) and quality (e.g., pore formation and delamination) of the built parts. The build quality is highly dependent on the process parameters such as laser energy density, the scanning speed and strategy, layer thickness, hatching spacing, environment, etc. (Chua, Ahn, and Moon 2017; Spears and Gold 2016; Gu et al. 2006). The parameter window dictates the complex physical phenomena and transients in the laser-material interaction zone and melt pool morphology, such as rapid heating, melting, cooling, evaporation of the materials and also potentially defect formation. For a desirable build quality in the LPBF process, a correct choice of parameter levels is primary (Chua, Ahn, and Moon 2017; Van Elsen 2007; Spears and Gold 2016). However, in practice, even though the process operates in a favourable parameter window — owing to highly nonlinear dynamic transformations that arise in the laser interaction zone, especially in keyhole regime — the LPBF processes are prone to defects (Everton et al. 2016; Tapia and Elwany 2014).

Implementing sensors around the process zone and the correlation between the data and the process behaviour enable a better process real-time feedback and understanding. Several sensors have been used for defect monitoring in real-time during the LPBF process (Everton et al. 2016; Tapia and Elwany 2014; Grasso et al. 2018; Yan et al. 2018). Predominantly high-speed imaging and thermal-based vision system have been reported in the literature (Mani et al. 2017). Sensing and monitoring the temperature field around the process zone using pyrometers have been investigated for a decade (Pavlov, Doubenskaia, and Smurov 2010; Furumoto et al. 2013; Kruth et al. 2007). The major advantage of pyrometers is that the process zone's temperature can be measured without physical contact and can be converted to a digital signal for further analysis and correlation. However, the downside of the sensors is twofold. First, owing to the melt pools occurring in sizes of 10-250 microns (Cheng et al.; Gong et al. 2014), they often lack spatial resolution, except if these imaging techniques are combined with suitable optics to retrieve the spatial

information from the melt pool morphology (Wang et al. 2017; Bayle and Doubenskaia 2008; Zhang et al. 2018; Clijsters et al. 2014). Second, only information about the surface can be detected, and understanding the mechanism beneath is unsolved at present. Though these imaging systems are a viable solution in AM monitoring, it is to be noted that they are not an economical solution in terms of cost, hardware and data management. Air and structure-borne acoustic emission (AE) based monitoring techniques for laser processing pose as an alternative and effective, low-cost solution for two main reasons (Shevchik et al. 2018; Masinelli, Shevchik, et al. 2020; Pandiyan et al. 2020). First, they are able to sense volumetric information of the process, e.g., melt pool fluctuation and keyhole instabilities leading to defect formation (Brandt 2016). Second, they have a high temporal resolution suitable to monitor melt pool events on a time scale between roughly 10 to 100 μs (Khairallah et al. 2016; Fisher et al. 2018; Zhao et al. 2017). However, due to the 3D nature of acoustic waves, the sensors' installation in terms of location, distance, angle, and filtering must be crucially ensured. The AE sensing element's proximity and positioning are directly proportional to sensitivity and signal strength from the source, which will impact the decision making. The portability of AE sensing across the different configuration of LPBF requires these factors to be considered. From an industrialization and commercialization perspective, installing an AE monitoring system requires minimum alteration to the existing machines available in the market [29], which gives an edge over other sensing techniques.

Real-time monitoring, defect detection, and subsequent counteractive measures have been proven to be efficient for LPBF processes when the sensor data is analysed with Machine Learning (ML) algorithms. ML methods, indeed, are capable of recognizing patterns and correlations hidden in the sensors data. A comprehensive review of supervised, semi-supervised, unsupervised, and reinforcement learning techniques applied in monitoring the AM processes has been reported by Goh e*t al.,* Meng e*t al.* and Sing e*t al.* (Goh, Sing, and Yeong 2021; Meng et al. 2020; Sing, Kuo, et al. 2021). Gaussian Mixture Models (GMM) have also been proven to identify the build quality using randomized Singular Value Decomposition (SVD) features extracted from a photodiode sensor (Okaroa et al. 2018). Luke Scime and Jack Beuth proposed computer vision algorithms trained on the powder bed images to automatically detect and classify anomalies during the powder spreading process (Scime and Beuth 2018a, 2018b). Different Convolutional Neural Networks (CNN) architectures and ML algorithms have been successfully applied in classifying the quality of the build, melt states and melt-pool morphology using melt-pool imaging (Kwon et al. 2020; Tan et al. 2019; Ye, Fuh, et al. 2018a; Gobert et al. 2018). Deep Learning (DL) algorithms have been able to effectively detect flaws in each layer using digital camera images compared to algorithms such *K*-nearest neighbour (KNN), logistic regression, SVM,

decision tree (DT), linear discriminant analysis (LDA), and boosted trees (BT) (Imani et al. 2019). Although, as mentioned, ML methods have implemented into AM processes in many ways in recent years, those methods have just started to be applied to bioprinting. Yu and Jiang (Yu and Jiang 2020) presented the perspective on the use of ML methods to improve 3D bioprinting whereas An et *al.* (An, Chua, and Mironov 2021) articulated the vision of future of 3D bioprinting via two missing links; big data and digital twin.

Several studies exist in a combination of ML algorithms with AE during the processing of metal-based materials with lasers for AM processes such as welding, direct energy deposition etc., to monitor and control the quality of the processes (Masinelli, Le-Quang, et al. 2020; Bastuck et al. 2015; Sumesh et al. 2015; Wasmer et al. 2018). With the feasibility of AE based monitoring proven in laser processing, there is a recent trend in the monitoring of the LPBF processes based on AE by exploiting state of the art ML algorithms. The linear SVM classifier was proven to be effective in classifying different processing regimes using statistical features computed on acoustic signals (Ye, Fuh, et al. 2018b). Shevchik *et al.* (Shevchik et al. 2019; Shevchik et al. 2018) successfully demonstrated that wavelet spectrograms computed on signals from optoacoustic fibre sensors corresponding to three porosity content could be classified with different CNN architectures Spectral CNN, Xception and ResNet. Deep belief networks have also been used to classify raw acoustic signals corresponding to defect patterns such as *balling*, normal and overheating (Ye, Hong, et al. 2018). Long short-term memory networks trained on AE have been able to detect process flaws such as keyhole porosity, lack of fusion, and bead up (Zhang et al.). Reinforcement learning approaches have also been combined with acoustic data for in situ quality monitoring (Wasmer et al. 2019). Structure-borne acoustic sensor data represented in the form of a spectrogram have been combined with neural networks to classify printed specimens' density in the LPBF process (Eschner et al. 2020). Most of the approaches discussed in material processing with lasers were based on a supervised learning paradigm. Semi-supervised CNN architectures for anomaly detection using AE signals in LPBF has been rarely reported in the literature (Goh, Sing, and Yeong 2021; Meng et al. 2020; Sing, Kuo, et al. 2021)., which will be bridged in this work.

Conventional supervised ML classification problems involve collecting datasets corresponding to each investigated process regime (e.g., balling, lack of fusion, conduction, keyhole). It is also important to have each dataset with equal weightage (a balanced database for each class) or otherwise requiring some compensation to be added during training to avoid biasing. Hence, developing and being aware of process maps for each class is a prerequisite before collecting the data. This is very time and material demanding and therefore expensive for industries. Also,

supervised classification models would not be able to classify new regimes from the trained ones if they are unfamiliar. It will classify the new regime into the class, which is statistically the closest. This may have dramatic consequences if the new mechanism decreases either the mechanical properties or the lifetime of the parts but is statistically close to the best regime. Under such a situation, the model has to be retrained again with the inclusion of data from the new class, increasing the cost of the process maps. A solution to this problem is using semi-supervised anomaly detection models, which are helpful in two main circumstances. First, when it is difficult, if not possible, to have a balanced dataset between the investigated regimes. This is particularly the case, for example, for machines or parts subjected to tribological failures (Shevchik et al. 2021). Most of the time, the process runs in the "normal" condition until an abrupt failure takes place. Second, when out of all the classes that are to be identified, only one is the most important or of interest. The semi-supervised models are trained only from the data distribution corresponding to the desired class, enabling the model to differentiate the data from which it was not trained. Works on monitoring the LPBF process using AE signatures reported so far have been more focused on discriminative models that are supervisedly trained. The novelty of the present work is on exploiting the generative models such as Variational autoencoder (VAE's) and General adversarial network (GAN's) trained semi-supervisedly to monitor the metal-based AM process. In this work, AE signals were acquired by a low-cost microphone during the process of the LPBF of a nickel-based super-alloy (Inconel 718) powder. The laser processes parameters were selected to produce parts of different qualities; a defect-free regime and three regimes containing defects. The main goals were to train two generative CNN models based on VAE and GAN with AE signals of the defect-free regime to detect anomalies (defects) such as *balling*, *LoF pores,* and *keyhole pores*.

The paper is organized into 5 Sections. Section 1 presents a succinct literature review of the LPBF process regimes, sensing techniques, and machine learning algorithms used for real-time process monitoring. Section 2 gives a brief overview of autoencoders and GAN. Section 3 describes the LPBF experimental setup, processing parameters, and data acquisition setup. Section 4 presents and discusses the anomaly prediction results using the AE signals emitted during LPBF by the two generative CNN architectures, such as VAE and GANomaly. Finally, Section 5 summarizes this investigation's findings and the future works on in situ monitoring for the LPBF process.

2 Theoretical basis

2.1. Variational Auto Encoder

Autoencoders and their variants find their applications predominant in image denoising (Gondara 2016), dimensionality reduction (Mahmud, Huang, and Fu 2020), feature extraction (Nishizaki 2017), image generation (Pandiyan et al. 2019; Cai, Gao, and Ji 2019), machine translation (Pagnoni, Liu, and Li 2018), and anomaly detection (Sakurada and Yairi 2014; Hahn and Mechefske 2021; Pandiyan et al. 2021). An autoencoder architecture generally consists of a pair of networks, namely an encoder and a decoder whose purpose is to learn the identity function for the data distribution they had been trained on. The encoder-decoder combination learns the data representation efficiently in a dense manner and reconstructs the original input. The encoder network maps the original data $x \in X$, to z belonging to low dimensional latent space Z using a function Φ. Subsequently, the decoder network recreates $x' \in X$ similar to the original data from z by a function Ψ, as depicted in Equations (1) and (2):

$$\Phi: X \rightarrow z, \qquad z = f(x, \Phi) \tag{1}$$

$$\Psi: z \rightarrow X, \qquad x' = f'(z, \Phi') \tag{2}$$

During training, the model learns to retain the minimal information to encode the original data X so that it can be regenerated as the output on the other side by back-propagating the reconstruction loss as presented in Equation (3), which is the difference between the input and output.

$$\mathcal{L}(x, x') = \|x - x'\|^2 = \|x - f'(f(x, \Phi), \Phi'))\|^2 \tag{3}$$

Once the autoencoder has been trained, we both have an encoder and a decoder to reconstruct the input. However, still, there are chances of overfitting as the latent space is not regularised, as illustrated in Figure 1(a). Variational autoencoder (VAE) is one of the types of autoencoders where latent space distribution is regularised during the training. The VAE provides a probabilistic manner for describing an observation in latent space. Thus, instead of building an encoder that outputs a single value to describe each latent state attribute, we will make our encoder define a probability distribution for each latent feature. In other words, the encoder does not directly map to the latent space

as depicted in Figure 1(a), instead it generates two quantities, mean (μ) and variance (σ^2) describing the distribution as shown in Figure 1(b) .

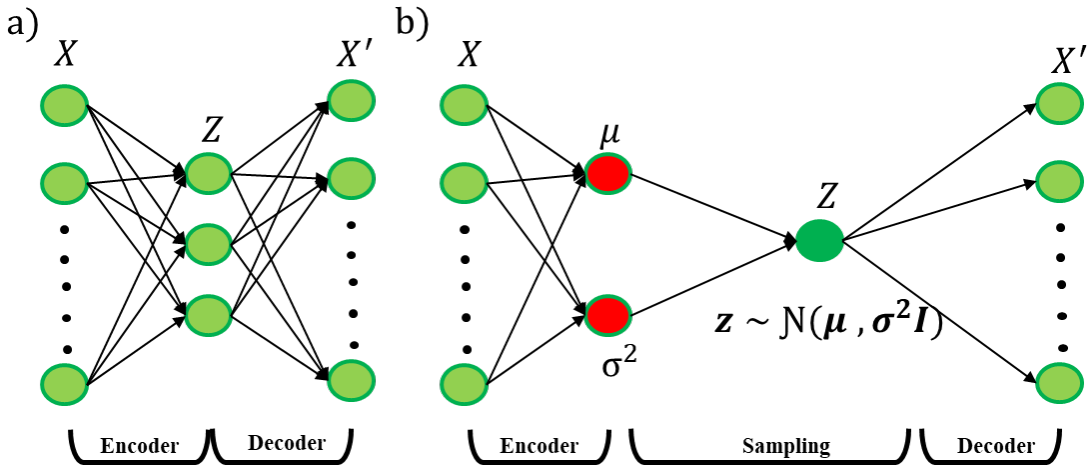

Figure 1. Illustration of (a) an autoencoder and (b) variational autoencoder architecture depicting latent space with and without regularisation.

Unlike vanilla autoencoders (An and Cho 2015), the loss function of the VAE network consists of two terms. The first term maximizes the reconstruction likelihood similar to Equation (3). The second term, also known as the Kullback–Leibler (KL) divergence, encourages the learned distribution *q(z|x)* to be identical to the true prior distribution *p(z)*, for each dimension *j* of the latent space as depicted in Equation (4). The KL divergence score ensures that the distribution learned *q* is similar to the true existing distribution *p*.

$$\mathcal{L}(x,\, x') = \|x\, - x'\|^2 + \sum_j KL(q_j\,(z|x) \,\|\, p(z)) \tag{4}$$

2.2. Generative Adversarial Network

A Generative Adversarial Network (GAN) is based on the idea that two adversarial networks, as shown in Figure 2, a generative network *G* and a discriminative network *D* that are set against one another during model training. The goal of the generative network's is to create new distribution samples that are different but still reminiscent enough from the training data. The goal of the discriminator network is to differentiate the synthetic distribution created by the generator network from the original training set.

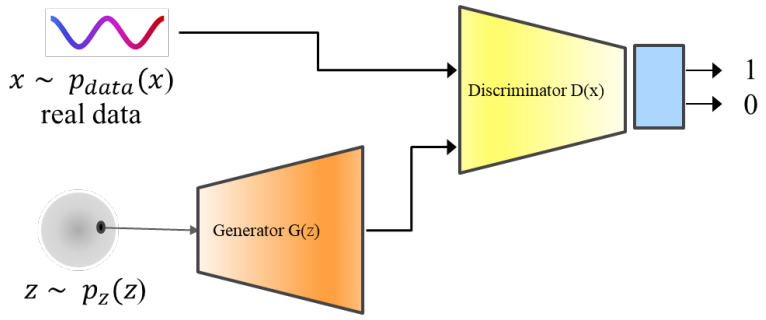

Figure 2. Illustration of a GAN architecture with generator network *G* and a discriminator network *D*.

Based on the set objective, the two networks iteratively improve during training such that the generator network is capable of creating synthetic data resembling the actual distribution. An example is presented in Figure 3.

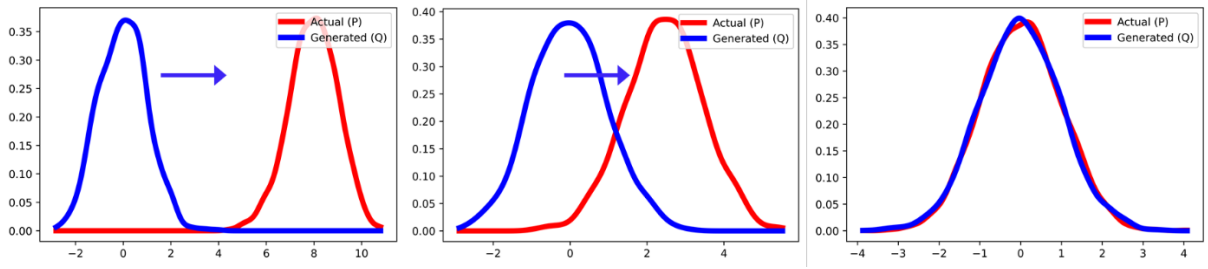

Figure 3. Comparisons of the distribution generated by the generator with training iteration with the actual distribution.

The training of the two networks requires a loss function, which primarily depends on the second network. The update of the weights does not occur simultaneously in the networks. The loss function for the vanilla GANs are of the form shown in Equation (5), where *D* is the discriminator, *G* is the generator, $p_z(z)$ is the input noise distribution, $p_{data}(x)$ is the original data distribution, and $p_g(x)$ is the generated distribution. The objective of the architecture is to maximize the discriminator (*D*) and minimize the generator (*G*). *V* is the sum of the Expected log-likelihoods for real and generated data. The loss function aims to move $p_g(x)$ towards $p_{data}(x)$ for an optimal *D*.

$$\min_G \max_D V(D, G) = \mathbb{E}_{x \sim p_{data}(x)} + \mathbb{E}_{z \sim p_z(z)}\left[\log(1 - D(G(z)))\right] \quad (5)$$

GANomalies are recent variants of the GAN network architectures where — based on known input — the network would generate a manifold representation of the input. However, when unusual input is encoded, its

reconstruction can be poor, which can be used for anomaly detection. GANomaly (Akcay, Atapour-Abarghouei, and Breckon 2018), AnoGan (Schlegl et al. 2019), and Efficient-GAN-Anomaly (Zenati et al. 2018) are the adversarial networks based on GAN architecture for identifying anomalies and outliers.

3 Experimental setup

3.1. Experimental setup and materials

The experimental setup, presented in Figure 4, consists of an enclosed chamber hosting a base plate, a recoater, and a laser. The laser operates in continuous mode at a 1070 ± 10 nm wavelength and has a spot size of 82 µm ($1/e^2$) with a beam quality with an $M^2 < 1.1$. The experiments were a series of overlapping lines track to build on a defect-free cube of the same material. The chosen scanning strategy was one-directional parallel lines with a hatch distance of 0.1 mm. The scanning speed and laser power were altered simultaneously to induce the four main process regimes (*balling*, *Lack of Fusion pores* (*LoF pores*), *conduction mode*, *keyhole pores*). The material used for the experiments was a nickel-based super-alloy known as Inconel 718. The powder was acquired from Oerlikon Metco, and its chemical composition is listed in Table 1. The size of the Inconel 718 powder particles used in this study varied between 15 and 45 µm and followed a normal distribution. The combination of laser power and scanning velocity for the investigated process regimes *balling, LoF pores, conduction mode,* and *keyhole pores* is listed in Table 2. The occurrence of the four process regimes was confirmed by cross-section analysis. The samples were sectioned perpendicular to the scan direction and polished. The melt pool was revealed by etching with Kalling's No.2 Reagent (5 g CuCl, HCl 100 mL, C_2H_6O 100 mL, H_2O 100 mL) for 10 to 20 seconds. The cross-sections were inspected with a Leica DM6000M light optical microscope in bright field mode. The optical pictures acquired for the four regimes are shown in Figure 5. Based on the picture "no pores", the porosity of the built layer on the defect free cube was less than 0.01% in conduction regime.

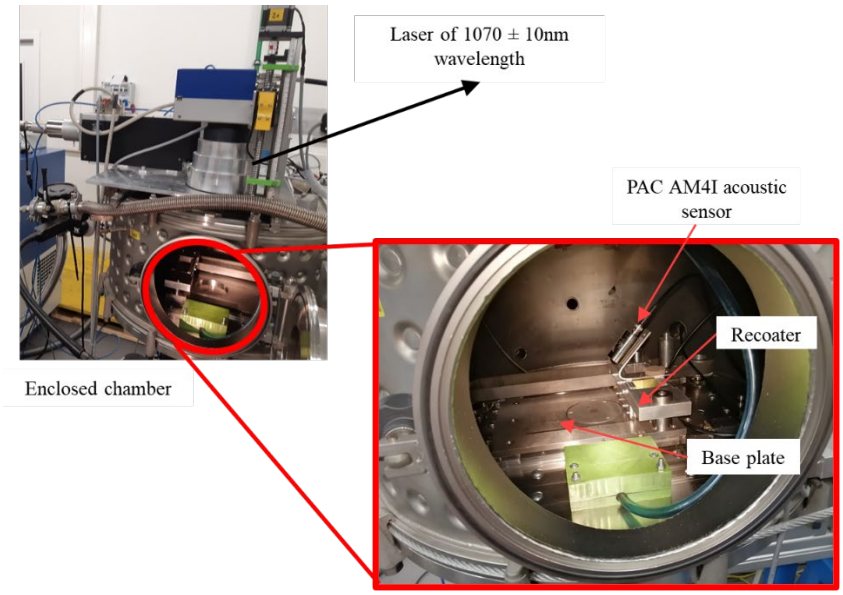

Figure 4.Customized LPBF experimental setup with the embedded acoustic sensor setup for anomaly detection.

Table 1. Chemical composition of the Inconel 718.

Ni	Ti	Cr	Mo	Nb+Ta	Fe	Al	Other
Balance	1	18	3	5	18	0.60	< 0.5

Table 2. Energy densities for line track experimental trials to induce the four regimes.

Categories	Laser power [W]	Scan speed [mm/s]	Normalized enthalpy (Ghasemi-Tabasi et al. 2020)
Balling	30	300	8.9
LoF pores	50	300	14.9
Conduction mode	120	300	35
Keyhole pores	450	200	164

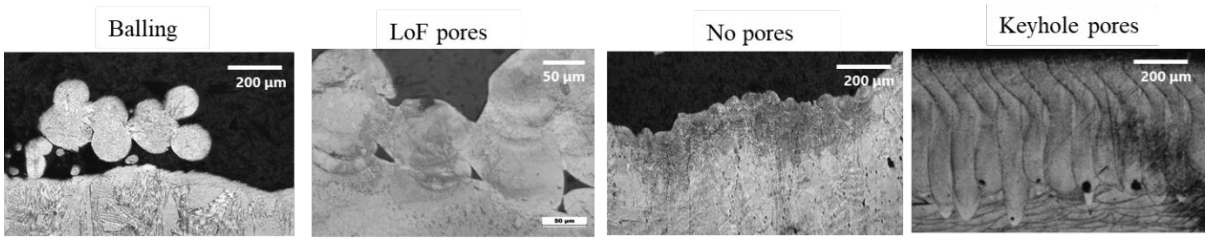

Figure 5. Optical pictures of different regimes such as *balling, LoF pores, conduction mode,* and *keyhole pores* occurring during LPBF of Inconel 718.

3.2. Data acquisition and dataset preparation

In this work, the airborne AE of the process zone was acquired with a PAC AM4I (Physical Instruments, US) airborne resonant acoustic sensor with an operating range of 0-100 kHz and Advantech Data Acquisition (DAQ) card. The AE sensor was fixed at a distance of more or less 5 cm from the process zone, as shown in Figure 4. The data acquisition rate of 1 MHz was chosen to ensure that the Nyquist Shannon theorem (Jerri 1977) is satisfied. The data acquisition was automatically triggered with a photodiode, and a schematic of the sensor setup is given in Figure 6. Owing to the 0-100 kHz sensor sensitivity range, an offline low-pass Butterworth filter with a cut-off frequency of 100 kHz is applied on the raw signal to omit noises. The raw signal corresponding to the four different process regimes is chopped into windows of 5ms (Pandiyan et al. 2020). Figure 7 presents the moving average plot of the normalized raw signals corresponding to all four process regimes. In building up an ML pipeline, emphasis should be made on the pre-processing of the signal based on the nature of the sensor used and the process environment. The data and codes for this work are present in the following repo (https://c4science.ch/diffusion/11519/).

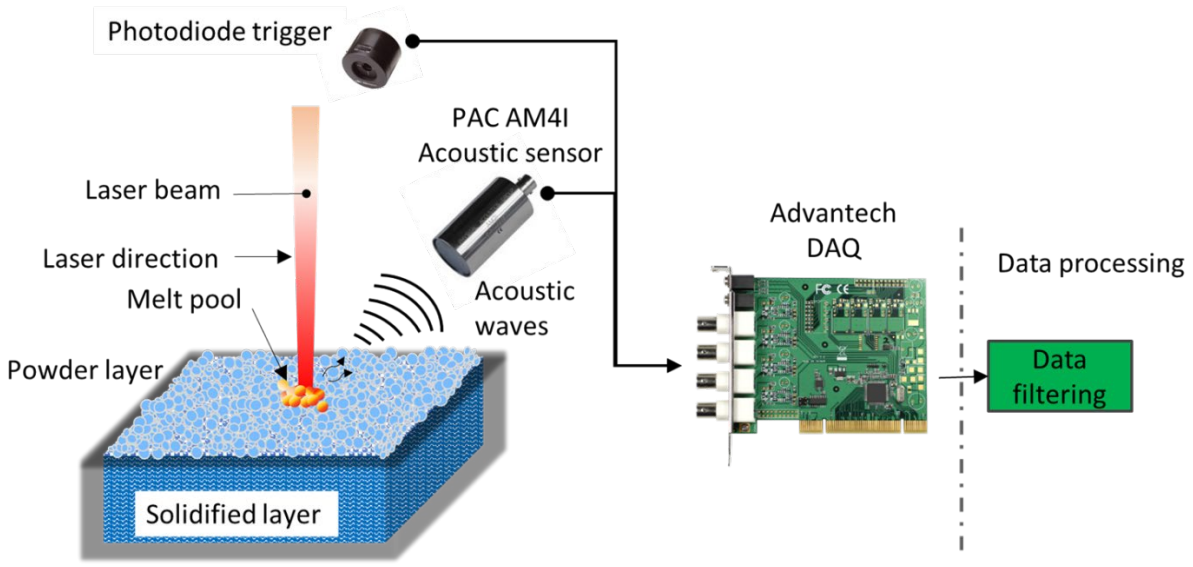

Figure 6. Schematic of the data acquisition pipeline with PAC AM4I acoustic sensor and photodiode trigger.

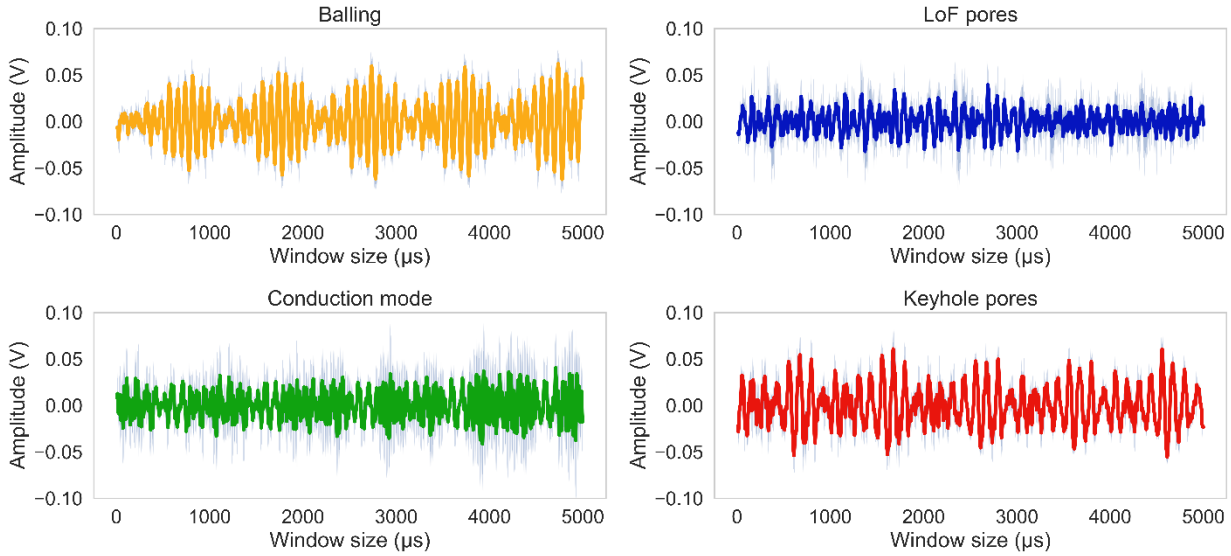

Figure 7. Normalized AE signals acquired of the four investigated process regimes, namely *balling*, *LoF pores*, *conduction mode,* and *keyhole pores*.

4 Anomaly detection

The primary idea of this work is to predict outliers or anomalies in the LPBF process based on acoustic emissions. The parts printed in the *conduction mode* regime are considered ideal conditions for the best mechanical properties. In contrast, each regime (*balling, LoF pores and keyhole pores*) is considered as process anomaly. Consequently, the acoustic signals from these regimes are grouped as anomalies, whereas the signals corresponding

to *conduction mode* are used for training the neural networks. The anomaly detection accuracy depends on understanding the "normal" data (AE signature from *conduction mode* in our case) so that abnormal data (AE signature from *balling, LoF pores,* and *keyhole pores* in our case) can be easily differentiated. Table 3 shows the dataset to train the two CNN architectures. The parameter inputs for training the two architectures, namely VAE and GANomaly, for identifying the anomalies, are listed in Table 4.

Table 3. Acoustic signal datasets for training and testing.

Class	**AM process regime**	**Samples of window size (5ms)**	**Training model**	**Testing model**
Normal	*Conduction mode*	2700	75% of the total sample	25% of the total sample
Anomaly / Outlier	*Balling, LoF pores* and *keyhole pores*	13680 (2730-*balling*, 2750- *keyhole pores*, 8200- *LoF pores*)	-	100% of the total sample

Table 4. Parameters used in VGG and ResNet Architectures for training.

Training parameters	**VAE**	**GANomaly**
Type of analysis	Anomaly detection	Anomaly detection
Solver name	'adam'	'adam'
Learn rate	0.001	0.001
Architecture	Encoder / Decoder architecture with 5 layers	Generator / Discriminator architecture with 5 layers
Momentum	0.9	0.9
Total Epochs	300	300
BatchSize	100	100
Shuffle	Every-epoch	Every-epoch
Batch normalization	True	True
Training set (*Conduction mode*)	AE signal corresponding to *conduction mode* with a window size of 5ms	AE signal corresponding to *conduction mode* with a window size of 5000 µs

Anomaly set	AE signal corresponding to *balling, LoF pores* and *keyhole* pores with a window size of 5ms	AE signal corresponding to *balling, LoF pores* and *keyhole* pores with a window size of 5 ms
Input tensor size	1 x 1 x 5000	1 x 1 x 5000
Loss function	Mean squared error (MSE) with KL divergence loss	Customized loss functions
GPU training	GeForce RTX 2080 Ti	GeForce RTX 2080 Ti
Dropout	0.2	0.2
Library	Pytorch	Pytorch
Training parameters	786736	892691

4.1. VAE based anomaly detection

The variational autoencoder architecture selected in this research consists of 10 layers with 5 layers corresponding to the encoder (*E*) and 5 layers corresponding to the decoder (*D*), as illustrated by Figure 8. The choice of the VAE design was to have good accuracy with a minimum number of parameters to train. The input to the network is a tensor of size 1x1x5000**,** which is the windowed acoustic signal of 5 ms corresponding to the *conduction mode* regime. The five-layer architecture of the encoder (*E*) compresses the raw acoustic signal into a latent space of the size of 1x256x10, sampled randomly from the training distribution via 1-Dimensional convolution, batch normalization, and *tanh* activation. The compressed latent space representation of the signal is then reconstructed to its original form by the decoder (*D*), whose architecture consisting of 5 layers. The decoder (*D*) architecture is an inverse of the encoder architecture with 1-Dimensional convolution replaced by the 1-Dimensional transpose convolution for upsampling. The overall architecture of the VAE is symmetrical, and evidence of this is in Figure 8. The VAE is trained with the combination of Adam as its optimizer with a batch size of 100, a dropout rate of 0.5, and a learning rate of 0.001 for 300 epochs. The training parameters were selected based on trial and error. At each epoch of the model training, the normal dataset is passed into the network. The reconstruction loss is back-propagated to alter the weights of the network for better performance. The variational autoencoder's loss function is the sum of the reconstruction loss, given by Mean Squared Error (MSE) with the KL divergence loss.

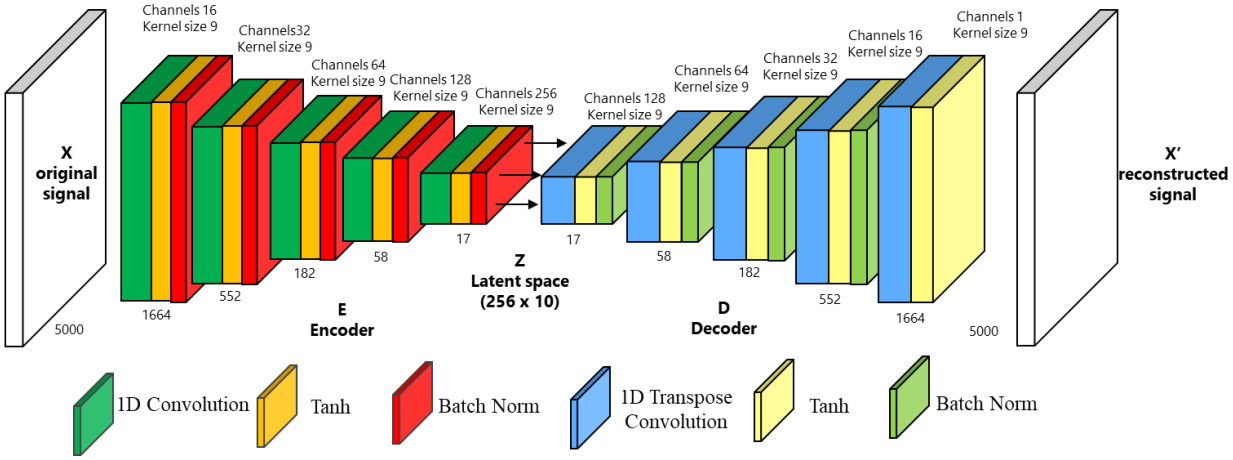

Figure 8. The architecture of the proposed variational autoencoder network.

Figure 9 represents the loss curves of the VAE model trained on raw acoustics signals corresponding to the *conduction mode* regime. From this figure, it is observed that the loss decreases with every epoch, confirming that the network learns the "normal" dataset patterns (*conduction mode*) and can reconstruct them efficiently. The saturation of the training loss with epochs suggests that the VAE network is trained.

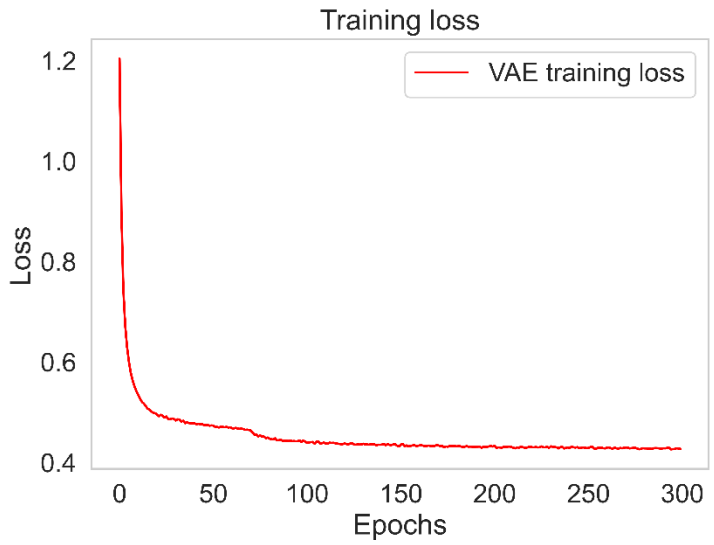

Figure 9. Training loss plot of VAE model on acoustic signals corresponding to *conduction mode* regime.

With the trained VAE network, the next step is to identify the reconstruction loss distribution on the "normal" dataset (*conduction mode* regime). Examining Figure 10(a), the maximum area of the reconstruction loss distribution lies in the range of 0 to 0.35 with a confidence of ≈ 95%. The threshold loss is calculated from the reconstruction distribution shown in Equation (6). We can define that any reconstruction loss corresponding to a signal more than the threshold value is classified as an anomaly.

$$Threshold = mean\ (\mu) + 3 \cdot standard\ deviations\ (\sigma) \quad (6)$$

Based on Equation (6), the threshold for anomaly detection for the trained VAE model has a value of 0.35, which is also synonymous with the visual examination. The VAE network's predictability is evaluated by comparing the reconstruction loss for each acoustic signal window in the anomaly dataset (*balling, LoF pores, and keyhole pores*) to the threshold value. The acoustic signals with reconstruction loss greater than threshold values are flagged as an anomaly. The reconstruction loss distribution of the *balling, LoF pores* and *keyhole pores* anomaly regimes are also plotted in Figure 10(b)-(d), respectively. It can be seen in Figure 10(b)-(d) that the reconstruction loss distribution density for the anomaly regimes are higher than 0.35. We can conclude that our proposed VAE architecture will differentiate normal conditions from other undesirable events for the selected time window from the reconstruction losses.

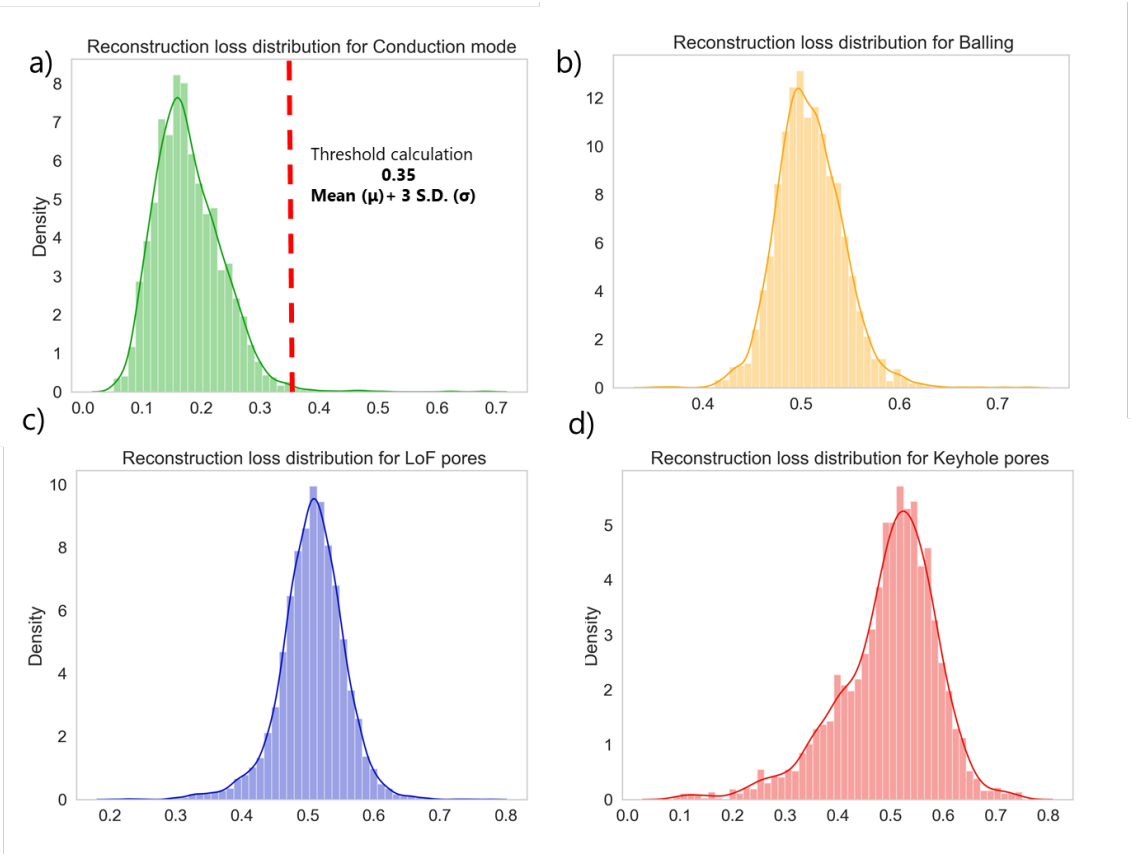

Figure 10. Distribution plots of reconstruction losses for normal and abnormal conditions.

The reconstructions of the VAE model on the acoustic signals corresponding to the "normal" conditions (the *conduction mode* regime) are presented in Figure 11(a). In this figure, the VAE model can recreate the true signal envelopes and patterns for the *conduction mode* regime. However, the reconstruction is pretty poor for the acoustic signals corresponding to the anomalies, and evidence of this is by the reconstruction losses in Figure 11(b). To achieve a statistically sound conclusion, we tested our approach on a total of 2100 windows (each 5 ms) corresponding to anomalies (700 each of *balling, LoF pores* and *keyhole pores*) and 700 windows (each 5 ms) corresponding to the normal regime. The trained VAE model correctly classified 2690 signal windows out of the 2800 windows giving an accuracy rate higher than 96% compared with the ground-truth labels.

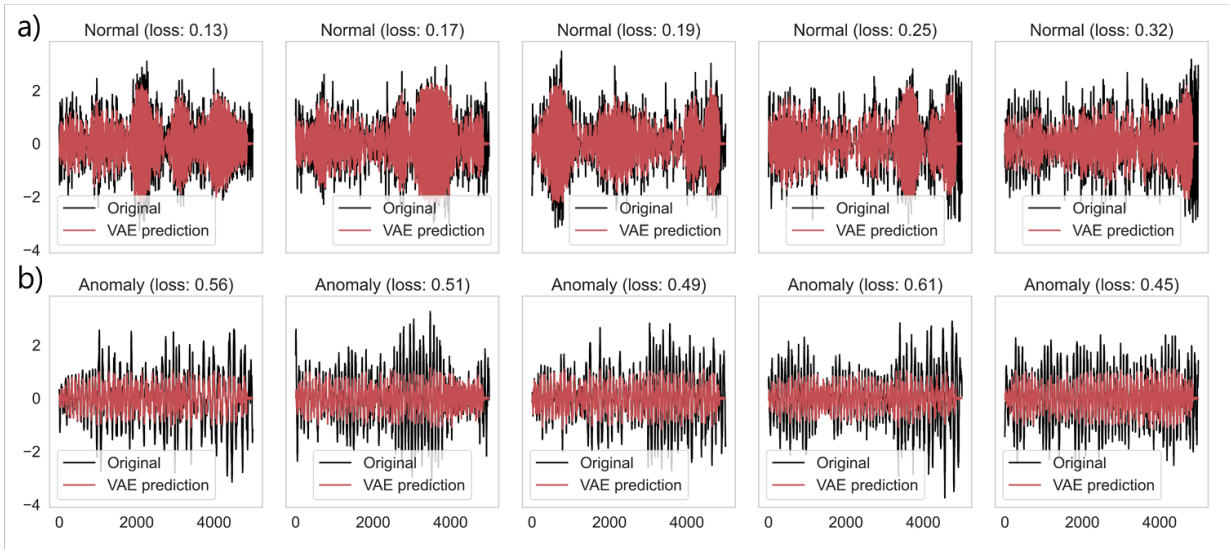

Figure 11. Reconstructions of the VAE model on (a) the "normal" and (b) the anomaly conditions.

4.2. GANomaly based anomaly detection

The signal analysis procedure for the GANomaly network is identical to VAE, and so only a summary is given here. The GANomaly network is trained on the acoustic signals corresponding to the *conduction mode* regime during training. Once trained, its parametrization is not suitable for generating distributions different from the trained samples. As a result, anomalies can be identified. The GANomaly architecture used in this work is inspired by the work of Akcay *et al.* (Akcay, Atapour-Abarghouei, and Breckon 2018).

Figure 12 is a schematic of the GANomaly architecture for time-series anomaly detection. The GANomaly model contains two encoders (G_{E1}, G_{E2}), a decoder (G_D), which forms the generator (G) and discriminator (D) network. The generator (G) learns the input data representation of the "normal" time-series signal distribution and reconstructs the signal via the use of an encoder (G_{E1}) and a decoder (G_D) network combination. Owing to the symmetrical VAE encoder-decoder architecture performance discussed in Section 4.1, the same layers and kernel filters are exploited to build the generator part. The second encoder (G_{E2}) design, a part of the generator, is a replica of the first encoder (G_{E1}). The encoder (G_{E1}) network downsamples the raw acoustic signal into a latent representation of size 1x256x10, and the decoder (G_D) network reconstructs the original signal from the latent space. The second encoder (G_{E2}) of the generator part compresses the reconstructed time-series signal into a latent size of 1x 256x 10. The discriminator (D) network plays the role of identifying fake and real signals like vanilla GANs. The GANomaly architecture is trained with adam optimizer with a batch size of 100, a drop out rate of 0.2, and a learning rate of 0.01 for 300 epochs similar

to VAE training parameters. At each epoch of the model training, *the conduction mode* dataset is passed into the network, and the computed loss is back-propagated to alter the network's weights for better performance. The loss function used for the training is a cumulative sum of three losses function as given in Equation (7).

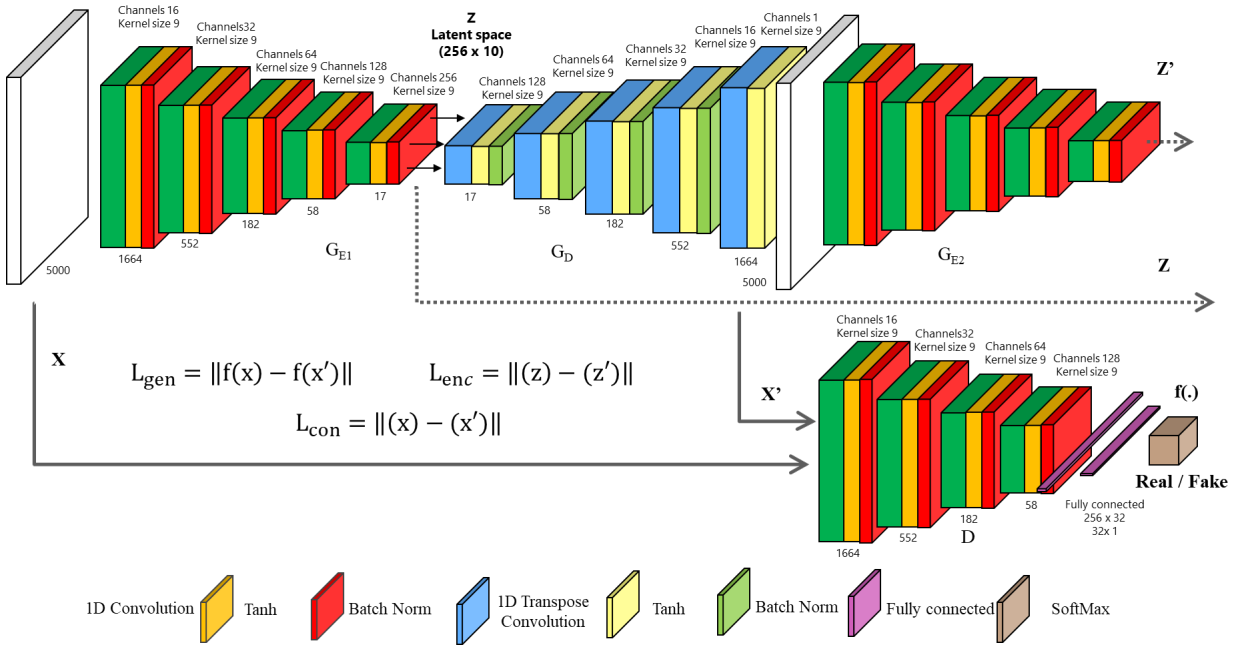

Figure 12. The architecture of the proposed GANomaly network comprising the generator and discriminator.

$$\text{Loss} = \omega_{con}.L_{con} + \omega_{enc}.L_{enc} + \omega_{gen}.L_{gen}$$

$$\text{Where, } L_{gen} = \|f(x) - f(x')\|, L_{enc} = \|(z) - (z')\| \text{ and } L_{con} = \|(x) - (x')\| \quad (7)$$

The construction loss (L_{con}) penalizes the generator as it is the MSE between the original sample *x* and the reconstructed one (*x' = G(x)*). The encoder loss (L_{enc}) is an additional loss minimizing the distance between the bottleneck features of the input ($z = G_E(x)$) and the encoded features of the generated image ($z' = E(G(x))$). Finally, the discriminator loss (L_{gen}) is the distance between the feature representation of the original acoustic signal and the generated signal. Unlike traditional vanilla GANs, where the generator (G) is not updated by back-propagating the output of discriminator (D) (real/fake), in this case, we update the generator (G) based on the internal representation of discriminator (D). Apart from the losses, there are weights ($\omega_{con}, \omega_{enc}, \omega_{gen}$) that can be tuned to the loss terms, which gives flexibility for the training. The weight values used for $\omega_{con}, \omega_{enc}$ and ω_{gen} during training are 20, 5 and

1, which were down-selected based on exhaustive search. Figure 13 shows the three training loss curves for the GANomaly model trained on the raw acoustics signals. The plots indicate that all three losses decrease with every epoch, confirming that the network is learning the training dataset's representation.

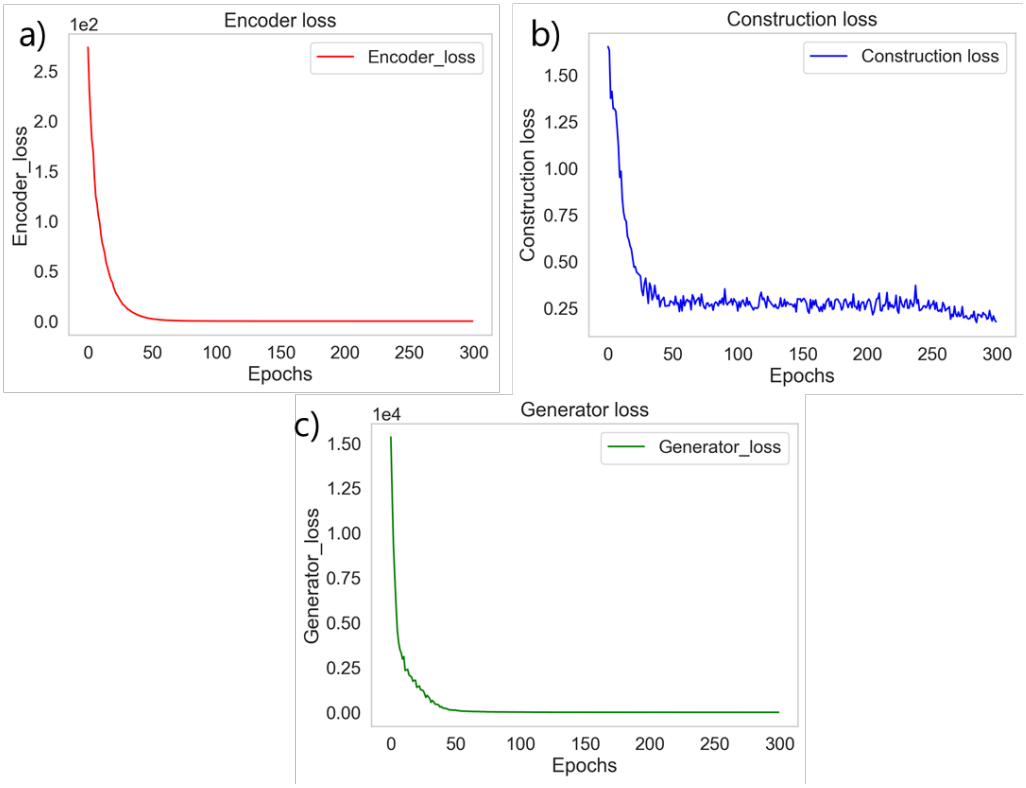

Figure 13. Training loss plot (a) Encoder loss, (b) Generator loss and (c) Construction loss of GANomaly model on acoustic signals corresponding to *conduction mode* regime.

After training the GANomaly, the next step is to identify the distribution of the reconstruction loss on the conduction mode dataset, similar to VAE, and the threshold value to flag the anomaly is calculated. Figure 14(a) is the distribution of the reconstruction loss for the *conduction mode* regime, and it is seen that it lies in the range of 0.0 to 0.22. With Equation (6), the threshold for anomaly detection is found to be 0.40. In other words, the reconstruction losses greater than the threshold value of 0.22 will be flagged as an anomaly. Figure 14(b) – (d) shows the reconstruction loss for each acoustic signal window in the anomaly datasets *balling, LoF pores* and *keyhole pores*, respectively. From these figures, it is seen that the reconstruction loss distribution of the anomaly regimes is higher

than the threshold value of 0.22. Consequently, inferring from the reconstruction losses, we can conclude that the proposed GANomaly architecture will differentiate normal conditions from other undesirable events.

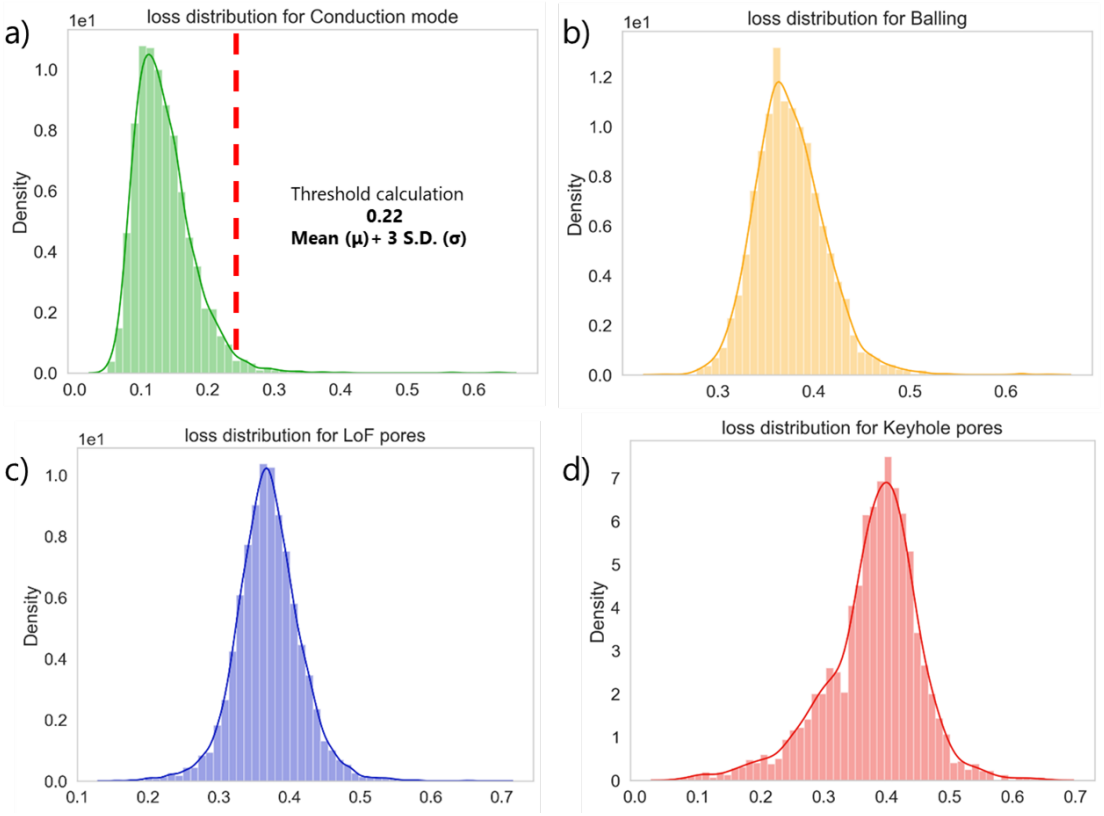

Figure 14. Distribution plots of reconstruction losses for normal and abnormal conditions.

Figure 15 presents the boxplot distribution of the losses predicted by the GANomaly model on the acoustic signals corresponding to the "normal" regime (*conduction mode* regime) and abnormal conditions (*balling, LoF pores* and *keyhole pores*). The plot shows that the losses for the trained *conduction mode* dataset are below the threshold of 0.22 as the parameterization are biased towards the distribution corresponding to the *conduction mode* dataset. A total of 2100 windows (each 5 ms) corresponding to anomalies (700 each of *balling, LoF pores* and *keyhole pores*) and 700 windows (each 5 ms) corresponding to the normal regime were tested. The trained GANomaly model correctly classified 2720 signal windows out of the 2800 windows giving an accuracy rate higher than 97% compared with the ground-truth labels.

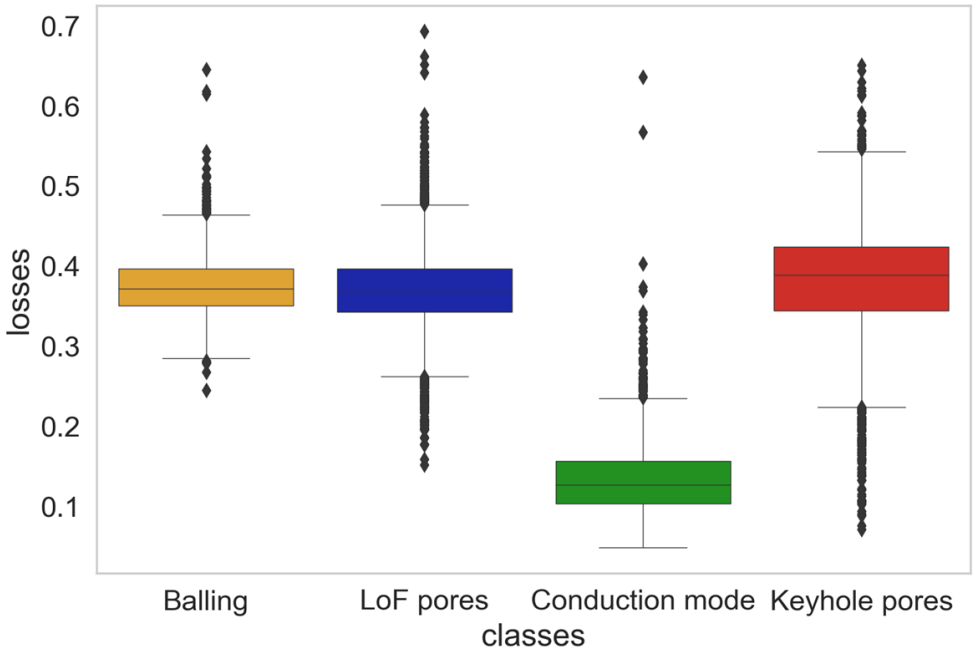

Figure 15. Box plots of reconstruction losses for normal and abnormal conditions confirm that the AE signal corresponding to anomaly regimes is greater than the threshold of 0.22.

4.3. Summary of the main results

Based on both the VAE and GANomaly models' prediction results, we demonstrated that the raw acoustic signals could be used as an input dataset to detect with high accuracy abnormal regimes such as *balling, LoF pores,* and *keyhole pores* occurring during LPBF processing of Inconel 718. VAE and GANomaly models distinguished the anomaly regimes such *balling, LoF pores, and keyhole pores* from the normal regime, i.e. *conduction mode*, with 96 and 97% accuracy. Comparing the two CNN architectures used in this study, it is found that the VAE performs slightly better in anomaly detection compared to GANomaly when the size of the network, trainable parameter, computational resource, and training time is taken as benchmarks and vice-versa if accuracy is taken into account.

5 Conclusions

We have demonstrated an approach based on semi-supervised methods to detect deviations from chosen qualities during the LPBF processes. In particular, based on the airborne acoustic signals from the process, the undesirable regimes, namely, *balling, LoF pores,* and *keyhole pores* could be differentiated from the reference regime *conduction*

mode. Two CNN architectures, VAE and GANomaly, were tested. The two models were trained on acoustic signals divided into windows of 5 ms corresponding to the *conduction mode* regime. These acoustic signals were captured during line track experiments on Inconel 718 in a customized LPBF setup. The sensor used in the study was an airborne resonant microphone with an operating range of 0–100 kHz. The data acquisition was made with an Advantech DAQ board at 1MHz. Based on the experimental results, the following generalized conclusions are drawn:

- Both the VAE and GANomaly models with symmetrical encoder-decoder architecture were able to detect undesirable regimes with ease. The GANomaly architecture with three losses and larger weights had better detection accuracy compared to VAE. Though GANomaly is a reasonably large network compared to the VAE architecture used in this work, it comes with a loss function that can be optimized during training to similar tasks on time-series signals.
- The two models' accuracy suggests that the reference regime's sensor signatures, i.e., defect regimes, can be differentiated from the too many ambiguous unfavourable regimes involved in the LPBF process with minimum effort spent on data collection and labelling.

The proposed approach establishes that the knowledge of LPBF processes on one regime in a material can be used to assess other regimes with minimum effort. The size of the Inconel 718 powder particles used in this study varied between 15 and 45 µm and followed a normal distribution. The laser-material interaction is affected by the powder characteristics, machine parameters and surface topography (Vock et al. 2019; Han et al. 2020; Sing, Huang, et al. 2021). Therefore trained GAN and VAE models cannot be generalized across different powder distributions, process parameters and alloying compositions. Though the models cannot be generalized, the VAE and GAN framework can be applied to process different powders with process map knowledge in Industrial LPBF setups to identify the abnormal regimes in a production environment. We have presented our work based on a window size of 5 ms, and the performance of the network in smaller window sizes is also a study in progress. The methodologies robustness in a more demanding situation where there are soft boundaries between anomaly and normal regimes is the planned research direction. As a final word, the optimization and fine-tuning of weights by adding skip connections in VAE architectures and performing a grid search to identify suitable weights for the loss function in GANomaly architecture will further optimize training and is also a part of future work. The data and codes for this work are present in the following repo (https://c4science.ch/diffusion/11519/).

Acknowledgement

The authors would like to acknowledge the financial support of the project MoCont from the program of the Strategic Focus Area Advanced Manufacturing (SFA-AM), a strategic initiative of the ETH Board. RDD and RL gratefully acknowledge the generous sponsoring of PX Group to their laboratory.

Funding

The authors would like to acknowledge the financial support of the project MoCont from the program of the Strategic Focus Area Advanced Manufacturing (SFA-AM), a strategic initiative of the ETH Board. RDD and RL gratefully acknowledge the generous sponsoring of PX Group to their laboratory.

Disclosure statement

The authors declare no conflict of interest.

Notes on contributors

Vigneashwara pandiyan is currently a Postdoctoral Researcher at Laboratory for Advanced Materials Processing, ETH Empa Swiss Federal Laboratories for Materials Science and Technology. He completed his Ph.D. from Nanyang Technological University, Singapore under Rolls-Royce @ NTU corp lab. He has 5+ years of experience as a researcher in manufacturing on characterization, investigation, optimization, and process development. Prior to joining Empa, he was a research scientist in A*Star - Agency for Science, Technology and Research ARTC, Singapore. He now concentrates on developing, validating, and implementing machine learning models for in-process sensing of manufacturing processes for anomaly detection and process automation based on sensor signatures.

Rita Drissi-Daoudi received her master degree in Mechanical Engineering in solid and structure mechanics with a minor in Material Sciences in 2018 from École Polytechnique Fédérale de Lausanne (EPFL). She is currently working toward her Ph.D. thesis on in-situ acoustic emission monitoring of the laser powder bed fusion process. at École

Polytechnique Fédérale de Lausanne (EPFL), at the Thermomechanical Metallurgy Laboratory, Her research includes signal processing and machine learning but is mainly emphasized on defects formation understanding and laser material processing

Sergey A. Shevchik received the master's degree in control from Moscow Engineering Physics Institute, Moscow, Russia, in 2003, and the Ph.D. degree in biophotonics from General Physics Institute, Moscow, in 2005. He was a Postdoctoral Researcher with General Physics Institute until 2009. Between 2009 and 2012, he was with Kurchatov Institute, Russia, developing image processing for human-machine interfaces. From 2012 to 2014, he was with the University of Bern, Bern, Switzerland, focusing on computer vision systems and multi-view geometry. Since 2014, he has been a Scientist with the Swiss Federal Laboratories for Material Science and Technology, Thun, Switzerland, developing signal processing and machine learning for industrial automatization. His research interests include signal processing and machine learning for industrial automatization.

Giulio Masinelli received the B.Sc. degree in electrical engineering from the University of Bologna, Bologna, Italy, in 2017, and the master's degree in electrical engineering from École Polytechnique Fédérale de Lausanne (EPFL), Lausanne, Switzerland, in 2019. He is currently working toward his Ph.D. thesis with EPFL and the Swiss Federal Laboratories for Material Science and Technology (Empa), Switzerland, mainly developing machine-learning algorithms for data analysis and industrial automation. His research interests include signal processing and machine learning with an emphasis on deep learning applied to embedded systems.

Tri Le-Quang received the B.S. degree in applied physics from Vietnam National University, Ho Chi Minh City, Vietnam, in 2007, the M.S. degree in optics from Friedrich-Schiller-Universität Jena, Germany, in 2013, and the Ph.D. degree in material engineering from the Instituto Superior Tecnico Lisboa, Portugal, in 2017. Since then, he has been holding a Postdoctoral position with the Laboratory of Advanced Materials Processing, Swiss Federal Laboratories for Materials Science and Technology (Empa). His research interests include laser material processing, laser technology, and in situ monitoring.

Roland Logé is a full-time professor currently working at the Materials Institute, École Polytechnique Fédérale de Lausanne (EPFL), Lausanne. Research activities are focused on the control and design of microstructures in metals and alloys through a combination of thermal and mechanical treatments. Phenomena of interest include recrystallization, grain growth, twinning, texture evolutions, precipitation, phase transformations, variable temperature conditions, and the possibility of concurrent plastic deformation. Different types of metal forming operations are investigated together with the selective laser melting process and its combination with laser shock peening.

Kilian Wasmer received the B.S. degree in mechanical engineering from Applied University, Sion, Switzerland, and Applied University, Paderborn, Germany, in 1999. He received the PhD degree in mechanical engineering from Imperial College London, London, U.K., in 2003. Since 2004, he has been with the Swiss Federal Laboratories for Materials Science and Technology (Empa), Thun, Switzerland, where he started to work on control of crack propagation in semiconductors. He currently leads the group of dynamical processes in the Laboratory for Advanced Materials Processing at Empa, Thun, Switzerland. Previously, he had focused his work on process development, process monitoring, and quality control via *in situ* and real-time observation of complex processes using acoustic and optical sensors in various fields such as in tribology, fracture mechanics, and laser processing. His research interests include materials deformation and wear, crack propagation prediction and material-tool interaction in particular laser material processing (e.g., welding, cutting, drilling, marking, cladding, additive manufacturing, etc.). Dr Wasmer is in the Director committee for additive manufacturing of Swiss Engineering. He is also a member of Swiss tribology, European Working Group of Acoustic Emission, Swissphotonics, and Deutsche Gesellschaft für Zerstörungsfreie Prüfung.

References

Akcay, Samet, Amir Atapour-Abarghouei, and Toby P Breckon. 2018. Ganomaly: Semi-supervised anomaly detection via adversarial training. Paper presented at the Asian conference on computer vision.

An, Jia, Chee Kai Chua, and Vladimir Mironov. 2021. "Application of Machine Learning in 3D Bioprinting: Focus on Development of Big Data and Digital Twin." *International Journal of Bioprinting* 7 (1).

An, Jinwon, and Sungzoon Cho. 2015. "Variational autoencoder based anomaly detection using reconstruction probability." *Special Lecture on IE* 2 (1):1-18.

Bastuck, Matthias, Hans-Georg Herrmann, Bernd Wolter, Peter-Christian Zinn, and Ralf-Kilian Zaeh. 2015. Acoustic in-process monitoring of laser welding. Paper presented at the International Congress on Applications of Lasers & Electro-Optics.

Bayle, F, and M Doubenskaia. 2008. Selective laser melting process monitoring with high speed infra-red camera and pyrometer. Paper presented at the Fundamentals of laser assisted micro-and nanotechnologies.

Brandt, Milan. 2016. "Laser additive manufacturing: materials, design, technologies, and applications."

Cai, Lei, Hongyang Gao, and Shuiwang Ji. 2019. Multi-stage variational auto-encoders for coarse-to-fine image generation. Paper presented at the Proceedings of the 2019 SIAM International Conference on Data Mining.

Cheng, Bo, James Lydon, Kenneth Cooper, Vernon Cole, Paul Northrop, and Kevin Chou. "Melt Pool Dimension Measurement In Selective Laser Melting Using Thermal Imaging Bo Cheng1, James Lydon2, Kenneth Cooper2, Vernon Cole3, Paul Northrop3, Kevin Chou1."

Chua, Zhong Yang, Il Hyuk Ahn, and Seung Ki Moon. 2017. "Process monitoring and inspection systems in metal additive manufacturing: Status and applications." *International Journal of Precision Engineering and Manufacturing-Green Technology* 4 (2):235-45.

Clijsters, Stijn, Tom Craeghs, Sam Buls, Karolien Kempen, and J-P Kruth. 2014. "In situ quality control of the selective laser melting process using a high-speed, real-time melt pool monitoring system." *The International Journal of Advanced Manufacturing Technology* 75 (5-8):1089-101.

Eschner, N, L Weiser, B Häfner, and G Lanza. 2020. "Classification of specimen density in Laser Powder Bed Fusion (L-PBF) using in-process structure-borne acoustic process emissions." *Additive Manufacturing* 34:101324.

Everton, Sarah K, Matthias Hirsch, Petros Stravroulakis, Richard K Leach, and Adam T Clare. 2016. "Review of in-situ process monitoring and in-situ metrology for metal additive manufacturing." *Materials & Design* 95:431-45.

Fisher, Brian A, Brandon Lane, Ho Yeung, and Jack Beuth. 2018. "Toward determining melt pool quality metrics via coaxial monitoring in laser powder bed fusion." *Manufacturing letters* 15:119-21.

Furumoto, Tatsuaki, Takashi Ueda, Mohd Rizal Alkahari, and Akira Hosokawa. 2013. "Investigation of laser consolidation process for metal powder by two-color pyrometer and high-speed video camera." *CIRP annals* 62 (1):223-6.

Ghasemi-Tabasi, Hossein, Jamasp Jhabvala, Eric Boillat, Toni Ivas, Rita Drissi-Daoudi, and Roland E Logé. 2020. "An effective rule for translating optimal selective laser melting processing parameters from one material to another." *Additive Manufacturing* 36:101496.

Gobert, Christian, Edward W Reutzel, Jan Petrich, Abdalla R Nassar, and Shashi Phoha. 2018. "Application of supervised machine learning for defect detection during metallic powder bed fusion additive manufacturing using high resolution imaging." *Additive Manufacturing* 21:517-28.

Goh, GD, SL Sing, and WY Yeong. 2021. "A review on machine learning in 3D printing: Applications, potential, and challenges." *Artificial Intelligence Review* 54 (1):63-94.

Gondara, Lovedeep. 2016. Medical image denoising using convolutional denoising autoencoders. Paper presented at the 2016 IEEE 16th International Conference on Data Mining Workshops (ICDMW).

Gong, Haijun, Hengfeng Gu, Kai Zeng, JJS Dilip, Deepankar Pal, Brent Stucker, Daniel Christiansen, Jack Beuth, and John J Lewandowski. 2014. Melt pool characterization for selective laser melting of Ti-6Al-4V pre-alloyed powder. Paper presented at the Solid freeform fabrication symposium.

Grasso, M, AG Demir, B Previtali, and BM Colosimo. 2018. "In situ monitoring of selective laser melting of zinc powder via infrared imaging of the process plume." *Robotics and Computer-Integrated Manufacturing* 49:229-39.

Gu, DD, YF Shen, JL Yang, and Y Wang. 2006. "Effects of processing parameters on direct laser sintering of multicomponent Cu based metal powder." *Materials science and technology* 22 (12):1449-55.

Guessasma, Sofiane, Weihong Zhang, Jihong Zhu, Sofiane Belhabib, and Hedi Nouri. 2015. "Challenges of additive manufacturing technologies from an optimisation perspective." *International Journal for Simulation and Multidisciplinary Design Optimization* 6:A9.

Hahn, Tim Von, and Chris K Mechefske. 2021. "Self-supervised learning for tool wear monitoring with a disentangled-variational-autoencoder." *International Journal of Hydromechatronics* 4 (1):69-98.

Han, Changjun, Qihong Fang, Yusheng Shi, Shu Beng Tor, Chee Kai Chua, and Kun Zhou. 2020. "Recent advances on high-entropy alloys for 3D printing." *Advanced Materials* 32 (26):1903855.

Imani, Farhad, Ruimin Chen, Evan Diewald, Edward Reutzel, and Hui Yang. 2019. "Deep learning of variant geometry in layerwise imaging profiles for additive manufacturing quality control." *Journal of Manufacturing Science and Engineering* 141 (11).

Jerri, A. J. 1977. "The Shannon sampling theorem—Its various extensions and applications: A tutorial review." *Proceedings of the IEEE* 65 (11):1565-96. doi: 10.1109/PROC.1977.10771.

Khairallah, Saad A, Andrew T Anderson, Alexander Rubenchik, and Wayne E King. 2016. "Laser powder-bed fusion additive manufacturing: Physics of complex melt flow and formation mechanisms of pores, spatter, and denudation zones." *Acta Materialia* 108:36-45.

Khajavi, Siavash H, Jouni Partanen, and Jan Holmström. 2014. "Additive manufacturing in the spare parts supply chain." *Computers in Industry* 65 (1):50-63.

King, Wayne E, Andrew T Anderson, Robert M Ferencz, Neil E Hodge, Chandrika Kamath, Saad A Khairallah, and Alexander M Rubenchik. 2015. "Laser powder bed fusion additive manufacturing of metals; physics, computational, and materials challenges." *Applied Physics Reviews* 2 (4):041304.

Kruth, Jean-Pierre, Peter Mercelis, Jonas Van Vaerenbergh, and Tom Craeghs. 2007. Feedback control of selective laser melting. Paper presented at the Proceedings of the 3rd international conference on advanced research in virtual and rapid prototyping.

Kwon, Ohyung, Hyung Giun Kim, Min Ji Ham, Wonrae Kim, Gun-Hee Kim, Jae-Hyung Cho, Nam Il Kim, and Kangil Kim. 2020. "A deep neural network for classification of melt-pool images in metal additive manufacturing." *Journal of intelligent Manufacturing* 31 (2):375-86.

Mahmud, Mohammad Sultan, Joshua Zhexue Huang, and Xianghua Fu. 2020. "Variational Autoencoder-Based Dimensionality Reduction for High-Dimensional Small-Sample Data Classification." *International Journal of Computational Intelligence and Applications* 19 (01):2050002.

Mani, Mahesh, Brandon M Lane, M Alkan Donmez, Shaw C Feng, and Shawn P Moylan. 2017. "A review on measurement science needs for real-time control of additive manufacturing metal powder bed fusion processes." *International Journal of Production Research* 55 (5):1400-18.

Masinelli, Giulio, Tri Le-Quang, Silvio Zanoli, Kilian Wasmer, and Sergey A Shevchik. 2020. "Adaptive Laser Welding Control: A Reinforcement Learning Approach." *IEEE Access* 8:103803-14.

Masinelli, Giulio, Sergey A Shevchik, Vigneashwara Pandiyan, Tri Quang-Le, and Kilian Wasmer. 2020. Artificial Intelligence for Monitoring and Control of Metal Additive Manufacturing. Paper presented at the International Conference on Additive Manufacturing in Products and Applications.

Meng, Lingbin, Brandon McWilliams, William Jarosinski, Hye-Yeong Park, Yeon-Gil Jung, Jehyun Lee, and Jing Zhang. 2020. "Machine learning in additive manufacturing: A review." *JOM* 72 (6):2363-77.

Nishizaki, Hiromitsu. 2017. Data augmentation and feature extraction using variational autoencoder for acoustic modeling. Paper presented at the 2017 Asia-Pacific Signal and Information Processing Association Annual Summit and Conference (APSIPA ASC).

Okaroa, Ikenna A, Sarini Jayasingheb, Chris Sutcliffeb, Kate Blackb, Paolo Paolettia, and Peter L Greena. 2018. "Automatic Fault Detection for Selective Laser Melting using Semi-Supervised Machine Learning."

Pagnoni, Artidoro, Kevin Liu, and Shangyan Li. 2018. "Conditional variational autoencoder for neural machine translation." *arXiv preprint arXiv:1812.04405*.

Pandiyan, Vigneashwara, Rita Drissi-Daoudi, Sergey Shevchik, Giulio Masinelli, Roland Logé, and Kilian Wasmer. 2020. "Analysis of time, frequency and time-frequency domain features from acoustic emissions during Laser Powder-Bed fusion process." *Procedia CIRP* 94:392-7.

Pandiyan, Vigneashwara, Pushparaja Murugan, Tegoeh Tjahjowidodo, Wahyu Caesarendra, Omey Mohan Manyar, and David Jin Hong Then. 2019. "In-process virtual verification of weld seam removal in robotic abrasive belt grinding process using deep learning." *Robotics and Computer-Integrated Manufacturing* 57:477-87.

Pandiyan, Vigneashwara, Josef Prost, Georg Vorlaufer, Markus Varga, and Kilian Wasmer. 2021. "Identification of abnormal tribological regimes using a microphone and semi-supervised machine-learning algorithm." *Friction*:1-14.

Pavlov, M, M Doubenskaia, and I Smurov. 2010. "Pyrometric analysis of thermal processes in SLM technology." *Physics Procedia* 5:523-31.

Sakurada, Mayu, and Takehisa Yairi. 2014. Anomaly detection using autoencoders with nonlinear dimensionality reduction. Paper presented at the Proceedings of the MLSDA 2014 2nd Workshop on Machine Learning for Sensory Data Analysis.

Schlegl, Thomas, Philipp Seeböck, Sebastian M Waldstein, Georg Langs, and Ursula Schmidt-Erfurth. 2019. "f-anogan: Fast unsupervised anomaly detection with generative adversarial networks." *Medical image analysis* 54:30-44.

Scime, Luke, and Jack Beuth. 2018a. "Anomaly detection and classification in a laser powder bed additive manufacturing process using a trained computer vision algorithm." *Additive Manufacturing* 19:114-26.

———. 2018b. "A multi-scale convolutional neural network for autonomous anomaly detection and classification in a laser powder bed fusion additive manufacturing process." *Additive Manufacturing* 24:273-86.

Shevchik, SA, S Zanoli, F Saeidi, B Meylan, G Flück, and K Wasmer. 2021. "Monitoring of friction-related failures using diffusion maps of acoustic time series." *Mechanical Systems and Signal Processing* 148:107172.

Shevchik, Sergey A, Christoph Kenel, Christian Leinenbach, and Kilian Wasmer. 2018. "Acoustic emission for in situ quality monitoring in additive manufacturing using spectral convolutional neural networks." *Additive Manufacturing* 21:598-604.

Shevchik, Sergey A, Giulio Masinelli, Christoph Kenel, Christian Leinenbach, and Kilian Wasmer. 2019. "Deep learning for in situ and real-time quality monitoring in additive manufacturing using acoustic emission." *IEEE Transactions on Industrial Informatics* 15 (9):5194-203.

Sing, SL, S Huang, GD Goh, GL Goh, CF Tey, JHK Tan, and WY Yeong. 2021. "Emerging metallic systems for additive manufacturing: In-situ alloying and multi-metal processing in laser powder bed fusion." *Progress in Materials Science*:100795.

Sing, SL, CN Kuo, CT Shih, CC Ho, and CK Chua. 2021. "Perspectives of using machine learning in laser powder bed fusion for metal additive manufacturing." *Virtual and physical prototyping*:1-15.

Spears, Thomas G, and Scott A Gold. 2016. "In-process sensing in selective laser melting (SLM) additive manufacturing." *Integrating Materials and Manufacturing Innovation* 5 (1):16-40.

Sumesh, A, Dinu Thomas Thekkuden, Binoy B Nair, K Rameshkumar, and K Mohandas. 2015. Acoustic signature based weld quality monitoring for SMAW process using data mining algorithms. Paper presented at the Applied Mechanics and Materials.

Tan, Yingshui, Baihong Jin, Alexander Nettekoven, Yuxin Chen, Yisong Yue, Ufuk Topcu, and Alberto Sangiovanni-Vincentelli. 2019. An encoder-decoder based approach for anomaly detection with application in additive manufacturing. Paper presented at the 2019 18th IEEE International Conference On Machine Learning And Applications (ICMLA).

Tapia, Gustavo, and Alaa Elwany. 2014. "A review on process monitoring and control in metal-based additive manufacturing." *Journal of Manufacturing Science and Engineering* 136 (6).

Van Elsen, Maarten. 2007. "Complexity of Selective Laser Melting: a new optimisation approach."

Vock, Silvia, Burghardt Klöden, Alexander Kirchner, Thomas Weißgärber, and Bernd Kieback. 2019. "Powders for powder bed fusion: a review." *Progress in Additive Manufacturing* 4 (4):383-97.

Wang, Di, Shibiao Wu, Fan Fu, Shuzhen Mai, Yongqiang Yang, Yang Liu, and Changhui Song. 2017. "Mechanisms and characteristics of spatter generation in SLM processing and its effect on the properties." *Materials & Design* 117:121-30.

Wasmer, K, T Le-Quang, B Meylan, and SA Shevchik. 2019. "In situ quality monitoring in AM using acoustic emission: A reinforcement learning approach." *Journal of Materials Engineering and Performance* 28 (2):666-72.

Wasmer, K, T Le-Quang, B Meylan, F Vakili-Farahani, MP Olbinado, A Rack, and SA Shevchik. 2018. "Laser processing quality monitoring by combining acoustic emission and machine learning: a high-speed X-ray imaging approach." *Procedia CIRP* 74:654-8.

Yan, Zhaorui, Weiwei Liu, Zijue Tang, Xuyang Liu, Nan Zhang, Mingzheng Li, and Hongchao Zhang. 2018. "Review on thermal analysis in laser-based additive manufacturing." *Optics & Laser Technology* 106:427-41.

Ye, Dongsen, Jerry Ying Hsi Fuh, Yingjie Zhang, Geok Soon Hong, and Kunpeng Zhu. 2018a. "In situ monitoring of selective laser melting using plume and spatter signatures by deep belief networks." *ISA transactions* 81:96-104.

Ye, Dongsen, Geok Soon Hong, Yingjie Zhang, Kunpeng Zhu, and Jerry Ying Hsi Fuh. 2018. "Defect detection in selective laser melting technology by acoustic signals with deep belief networks." *The International Journal of Advanced Manufacturing Technology* 96 (5-8):2791-801.

Ye, DS, YHJ Fuh, YJ Zhang, GS Hong, and KP Zhu. 2018b. "Defects Recognition in Selective Laser Melting with Acoustic Signals by SVM Based on Feature Reduction." *MS&E* 436 (1):012020.

Yu, Chunling, and Jingchao Jiang. 2020. "A perspective on using machine learning in 3D bioprinting." *International Journal of Bioprinting* 6 (1).

Zenati, Houssam, Chuan Sheng Foo, Bruno Lecouat, Gaurav Manek, and Vijay Ramaseshan Chandrasekhar. 2018. "Efficient gan-based anomaly detection." *arXiv preprint arXiv:1802.06222*.

Zhang, Wentai, Brandon Abranovic, Jacob Hanson-Regalado, Can Koz, Bhavya Duvvuri, Kenji Shimada, Jack Beuth, and Levent Burak Kara. "Flaw Detection in Metal Additive Manufacturing Using Deep Learned Acoustic Features."

Zhang, Yingjie, Geok Soon Hong, Dongsen Ye, Kunpeng Zhu, and Jerry YH Fuh. 2018. "Extraction and evaluation of melt pool, plume and spatter information for powder-bed fusion AM process monitoring." *Materials & Design* 156:458-69.

Zhao, Cang, Kamel Fezzaa, Ross W Cunningham, Haidan Wen, Francesco De Carlo, Lianyi Chen, Anthony D Rollett, and Tao Sun. 2017. "Real-time monitoring of laser powder bed fusion process using high-speed X-ray imaging and diffraction." *Scientific reports* 7 (1):1-11.